QUANTITATIVE ACCURACY OF DIFFERENT SINGLE PHOTON EMISSION COMPUTED TOMOGRAPHY/COMPUTED TOMOGRAPHY (SPECT/CT) SYSTEMS WITH PHANTOMS USING Tc-99m AND I-131

MOAYED YOUSEF HASAN AL-QINNAH

UNIVERSITI SAINS MALAYSIA

2023

QUANTITATIVE ACCURACY OF DIFFERENT SINGLE PHOTON EMISSION COMPUTED TOMOGRAPHY/COMPUTED TOMOGRAPHY (SPECT/CT) SYSTEMS WITH PHANTOMS USING Tc-99m AND I-131

by

MOAYED YOUSEF HASAN AL-QINNAH

Thesis submitted in fulfillment of the requirements
for the degree of
Doctor of Philosophy

June 2023

ACKNOWLEDGEMENT

First, I'd like to thank my advisor, *Dr. Syahir Mansor*, for pushing me to pursue research and guiding me.

My parents, *Yousef Hasan* and *Salwa Said*, gave me full trust, encouragement, and unlimited patience. My brother *Murad Yousef* has continuously encouraged and supported me despite our distance.

My parents-in-law, *Dr. Wasef Marashdih* and *Mrs. Hind*, have always been there for me emotionally.

Lastly, I'd want to thank my soulmate *Zain Wasef* and my kids, *Owais, Salwa,* and *Salma*; without their support, I would have struggled to finish my dissertation.

TABLE OF CONTENTS

LIST OF FIGURES

Page

LIST OF TABLES

Page

LIST OF SYMBOLS

α	Alpha particle
B^-	Beta particle
β^+	Positron sub-atomic particle
EC	Electron Capture
Ci	Curie
Bq	Becquerel
mSv	millisievert
Z_{eff}	Effective atomic number
ρ	Mass density
μ	Linear Attenuation Coefficient
$\mathcal{R}$	Radon Transform
δ	Coordinate rotation
$T_{1/2}$	Half-life

LIST OF ABBREVIATIONS

1D	One-Dimensional
2D	Two-Dimensional
3D	Three-Dimensional
AC	Attenuation Correction
CDR	Collimator-Detector Response
COR	Centre of Rotation
CR	Contrast Ratio
CT	Computed tomography
CTAC	CT-derived Attenuation Correction
DEW	Dual Energy Window
EM	Expectation-maximization
FBP	Filtered Back Projection
FOV	Field of View
FT	Fourier Transform
FWHM	Full Width at Half Maximum
FWTM	Full Width at Tenth Maximum
HEGP	High Energy General Purpose
IR	Iterative Reconstruction
IV	Intravenously
LEGP	Low Energy General Purpose
LET	Linear Energy Transfer
LOR	Lines Of Response
LSF	Line Source Function
MEGP	Medium Energy General Purpose
MLEM	Maximum Likelihood Expectation Maximization

MTF	Modulation Transfer Function
NaI(Tl)	Thallium activated Sodium Iodide
NPV	Negative predictive value
OSEM	Ordered Subsets Expectation Maximization
PET	Positron Emission Tomography
PMTs	Photomultiplier Tubes
PPV	Positive predictive value
PSF	Point Spread Function
PVE-PVC	Partial Volume Effect and Partial Volume Correction
QC	Quality Control
ROI	Region of Interest
ROR	Radius Of Rotation
RR	Resolution Recovery
SC	Scatter Correction
SD	Standard Deviation
SPECT	Single Photon Emission Computed Tomography
TEW	Triple Energy Window
VOI	Volume Of Interest

KETEPATAN KUANTITATIF SISTEM PANCARAN FOTON TUNGGAL TOMOGRAFI BERKOMPUTER/TOMOGRAFI BERKOMPUTER (SPECT / CT) BERBEZA DENGAN FANTOM MENGGUNAKAN Tc-99M DAN I-131

ABSTRAK

Pengimejan pancaran foton tunggal berkomputer (SPECT) merupakan satu fungsi volumetrik yang melalui proses penghasilan imej dan teduhan, memberikan imej keratan rentas taburan keradioaktifan. Matlamat pengkuantitian mutlak adalah untuk mengukur keradioaktifan dalam isipadu sasaran dalam unit mutlak seperti becquerels. Walaupun ketepatan kuantitatif SPECT bertujuan untuk mengukur perbezaan ketara antara pengkuantitian daripada data SPECT yang dibina semula dan aktiviti dalam objek sasaran, untuk membantu membimbing banyak aplikasi, seperti dosimetri dalaman untuk pengiraan dos, anggaran, dan pengoptimuman. Oleh itu, untuk menjana imej fungsian kuantitatif yang boleh diulang pada pesakit yang sama pada pelbagai titik masa dan boleh dihasilkan semula di seluruh pusat dan pengimbas, rujukan pengkuantitian mutlak dengan pekali variasi yang rendah diperlukan untuk memastikan pengharmonian antara pelbagai vendor dan pusat. Projek ini bertujuan untuk menilai prestasi tiga sistem SPECT/CT di tiga pusat iaitu Institut Perubatan dan Pergigian Termaju (AMDI-USM), Hospital Universiti Sains Malaysia (HUSM), dan Hospital Besar Pulau Pinang (PGH), serta menilai tahap ralat dalam pengiraan aktiviti di pusat-pusat yang terlibat. Selain itu, matlamatnya adalah untuk menilai kestabilan faktor penentukuran sistem SPECT/CT di AMDI dalam tempoh enam bulan. Metodologi yang terlibat menggunakan General Electric Discovery NM/CT 670, Pro NM/CT 670, dan Siemens Symbia Intevo T16 untuk mendapatkan imej pelbagai fantom yang dipenuhi dengan pelbagai kepekatan keradioaktifan daripada homogen

silinder kepada fantom yang mensimulasikan organ-organ badan. Tahap aktiviti yang ditambah kepada setiap komponen direka untuk menghasilkan kiraan yang serupa dengan yang diperhatikan pada pesakit yang telah menjalani kajian SPECT. Percubaan dibuat untuk mewujudkan faktor penentukuran SPECT menggunakan sumber ^{99m}Tc dan ^{131}I dalam larutan cecair yang akan membolehkan nilai pengkuantitian aktiviti mutlak pengkuantitian berdasarkan imej SPECT yang dibina semula. Ketepatan kuantitatif anggaran aktiviti dalam sistem SPECT/CT di pusat AMDI dan HUSM menunjukkan perbezaan mutlak dalam ± 15% dengan penggunaan pembinaan semula 3D-OSEM dengan pampasan untuk faktor kemerosotan fizikal seperti pengecilan, penyebaran, dan resolusi. Selain itu, keputusan menunjukkan bahawa ketepatan kuantitatif pengambilan aktiviti di PGH dianggar kurang sebanyak 5% daripada nilai sebenar. Dari segi kestabilan SPECT/CT, pengukuran yang dihasilkan dalam tempoh enam bulan menghasilkan kebolehubahan sebanyak 2.76% dalam tempoh yang disiasat. Kesimpulan terakhir adalah bahawa cara terbaik untuk mencapai kuantitatif yang tepat dalam pengimejan SPECT adalah untuk membina semula semua imej menggunakan algoritma pembinaan semula lelaran yang merangkumi pembetulan pengecilan dan pembetulan penyebaran.

QUANTITATIVE ACCURACY OF DIFFERENT SINGLE PHOTON EMISSION COMPUTED TOMOGRAPHY/COMPUTED TOMOGRAPHY (SPECT/CT) SYSTEMS WITH PHANTOMS USING Tc-99m AND I-131

ABSTRACT

Single-photon emission computed tomography (SPECT) imaging is a volumetric functionality, by rendering and shading, provides cross-sectional images of radioactivity distribution. The goal of absolute quantification is to measure the radioactivity within a target volume in absolute units such as becquerels. Although SPECT quantitative accuracy is intended to quantify significant differences between quantification from the reconstructed SPECT data and the ground-truth activity in the target object, to help guide many applications, such as internal dosimetry for dose calculation, estimation, and optimisation. Therefore, to generate quantitative functional images that are repeatable in the same patient at multiple time points and reproducible across centres and scanners, an absolute quantification reference with a low coefficient of variation is needed to assure harmonisation among multi-vendors and multi-centres. This project aimed to evaluate the performance of three SPECT/CT systems installed at three centres: the Advanced Medical and Dental Institute (AMDI-USM), Hospital Universiti Sains Malaysia (HUSM), and Penang General Hospital (PGH), and to assess levels of error in the quantitation of activity at the centres involved. Furthermore, the aim is to evaluate the stability of the calibration factor of the SPECT/CT system at AMDI over a six-month period. The methodology involved using the General Electric Discovery NM/CT 670, Pro NM/CT 670, and Siemens Symbia Intevo T16 to obtain images of a range of phantoms filled with various concentrations of radioactivity, from cylindrical homogenous to phantoms that

simulate organs of the body. The levels of activity added to each component of the phantom were designed to produce counts similar to those observed in patients who had undergone SPECT studies. An attempt was made to establish a SPECT calibration factor using ^{99m}Tc and ^{131}I sources in liquid solution that would allow the derivation of absolute activity quantification values based on reconstructed SPECT images. The quantitative accuracy of activity estimation in SPECT/CT systems at AMDI and HUSM centres shows an absolute difference within ± 15% with application of 3D-OSEM reconstruction with compensation for physical degrading factors such as attenuation, scatter, and resolution. Also, the results showed that the quantitative accuracy of the activity uptake at PGH is underestimated by 5% of the true value. In terms of stability of SPECT/CT, the measurements generated over a six-month period resulted in a variability of 2.76% over the period investigated. The final conclusion is that the best way of achieving accurate quantitation in SPECT imaging is to reconstruct all images using an iterative reconstruction algorithm that includes attenuation correction and scatter correction.

CHAPTER 1

SCOPE AND CONTRIBUTION TO THE PROGRESS OF RESEARCH

1.1 Motivation

Our world is in three spatial dimensions (3D), and one is a temporal dimension (time). In this sense, the human body and internal organs are inherently volumetric anatomies and dynamic machines. Therefore, it is more prefect tracres to examine regional body physiology and chemistry, where there is always something more to be seen. Hence, in 1962, David Kuhl introduced emission reconstruction tomography (1). His method, supposed by Radon, states that image reconstruction from projection is possible (2)*"the value of a two-dimensional function at an arbitrary point is uniquely obtained by the integrals along the lines of all directions passing the point"*. However, this method later became known as single-photon emission computed tomography[1] (SPECT) and positron computed tomography (PET). It was extended to transmission X-ray scanning, known as computed tomography (CT).

SPECT is based on the fundamental principle of the decay of radioisotopes to to measure the spatial and temporal distribution of the isotope perfused in a patient's body. By using this principle, SPECT allows the acquisition of a physiological image and the reconstruction of a dynamic image of the organ's function. The mechanism is that gamma-emitting radioisotopes (γ-rays) labelled with certain molecules (to form a radiopharmaceutical) are injected into the patient's bloodstream and preferentially accumulated based on the metabolism-dependent of functional tissues. An gamma

[1] The phrase "single photon" indicates that one photon per decay. In SPECT, only one γ-ray is emitted per decay of the source isotope. In PET, an annihilation radiation yielding two γ-rays ($e^+e^- \rightarrow \gamma\gamma$).

camera is then used to detect, track, and record the photons flux, their energy, and their direction of origin. By using appropriate electronic circuits, a 2D projection of the radioactivity distribution in the object is obtained. By acquiring multiple planar projections at different angles around an axis of the object, the 3D spatial distribution of radioactivity is estimated.

X-ray computed tomography is based on the fundamental principle of linear attenuation coefficients to image the distribution of attenuation inside the body. By this principle, CT allows the acquisition of anatomical images and the reconstruction of the body's density. The mechanism is that a flux of X-rays transmitted continuously through a full scan of the body are attenuated differently depending on the atomic number and density of the object. A multi-detector array on the opposite side detected the attenuated flux and stored it digitally by a sinogram format (data in raw). The reconstruction of a 2D slice is computed from the set of 1D projections collected from many angles around that slice. The 3D volume is then obtained by stacking on top of each other the reconstructed 2D slices that acquired from multiple axial slices at slightly offset locations. Thus, the computer uses complex mathematical algorithms to reconstruct the distribution of the object density.

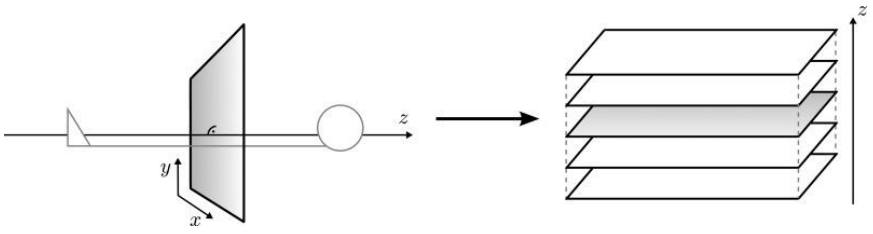

Figure 1.1 A 3D image of the body is formed by stacking 2D image slices in axial direction (3).

Multi-modality imaging using functional SPECT and morphological CT in a quasi-simultaneous acquisition on the same imaging instrument overcomes the

limitations of each alone. For instance, SPECT alone makes it difficult to precisely locate tracer uptake because it contains relatively high levels of statistical noise caused by a photon-limited process in which radionuclide imaging is extremely low photon flux, the need for a collimator that rejects a large number of photons that are both primary and scattered photons, the majority of γ-rays emitted during data acquisition do not travel in the direction allowed by the collimator therefore do not contribute to image formation, and there is a limited axial field of view that limits the anatomic region that can be scanned (4,5). In contrast, the most significant drawback of CT is that it does not give histological evidence or represent the functional and metabolic activity of the tissues since no pathological changes in morphology are present (6).

SPECT/CT is now commercially accessible and has served as proof of concept. It has been possible for the functional processes to be localised within the body by anatomical identification. In clinical studies, integration of multi-slice spiral CT into SPECT allows mapping of electron density distributions to generate an attenuation map to compensate for the inherent limitations of emission imaging and an anatomical orientation map to improve identification of focal points of abnormal tracer uptake and differentiation of pathologic from physiologic findings (7). Furthermore, CT provide a mass-density map for voxel-level dose-rate map calculation, which is primarily beneficial in targeted radionuclide therapy (TRT) and peptide receptor radiation therapy (PRRT) (8,9). Therefore, moving from 2D planar imaging to hybrid SPECT/CT imaging, further advancements in new image reconstruction algorithms culminated in the development of new techniques that compensate for the inherent limitations of SPECT imaging, provided superior quantification of activity uptake estimation, and added new clinical applications to the SPECT/CT portfolio.

1.2 Problem Statement

The use of standard procedures or protocols to measure the functional and metabolic behaviour of a lesion is valuable in the assessment of disease progression or follow-up studies monitoring disease response to treatments (10,11). Quantitative SPECT/CT can be used to gain a greater understanding of why certain subgroups of patients do not respond, for example, to radionuclide therapy. It can also be used to aid clinical development by determining the optimal activity to administer to each patient. In this manner, the European Association of Nuclear Medicine (EANM) in 2010, introduced "programme guidelines[2]" for the accreditation of PET/CT scanners using FDG, but such criteria have not yet been established for quantitative SPECT/CT imaging and still need to be demonstrated (12,13). Thus, it is important to define how to effectively implement quantitative SPECT/CT in order to offer a stable understanding of quantitative SPECT/CT. Numerous uncertainties and variable factors may be seen in SPECT, making standardized quantitative SPECT imaging across sites and centers hinder repeatable and reproducible measurements and need significant prior steps.

While there are three major commercial SPECT/CT systems on the market, namely: Siemens Symbia Intevo T16, Philips BrightView XCT, and General Electric Discovery NM/CT 670. Table 1.1 shows the characteristics of the three systems and their own 3D reconstruction algorithms. However, each of these manufacturing

[2] The programme runs within the scope of EANM Research Limited (EARL) activities. This broadly agreed guideline, amended to version 2.0 in 2014, aims to harmonise quantification in multi-centre studies and provide a minimum standard for the acquisition of PET/CT scans obtained with FDG.

systems has its own software-based algorithm for 3D iterative reconstruction with different correction techniques for attenuation correction, scatter correction, and resolution recovery (14–16). Also, the system resolution and detective quantum efficiency vary by vendor due to the neutral hardware-based design (17). In clinical practise, institute-specific settings include system calibration and projection and reconstruction parameters (e.g., number of iterations and subsets, post-filtering) that are not the same (18). Accordingly, clinical users should be aware that the same patient may have different clinical imaging outcomes if scanned by several SPECT/CT systems at different sites. As a result, quantitative SPECT/CT, like PET/CT, is in high demand (12,13).

Recent research has evaluated the clinical utility of quantitative SPECT/CT in multi-center and intra-vendor systems. Table 1.2 shows the major studies that evaluated the accuracy of absolute activity quantification in SPECT/CT among different scanners and centers. In 2002, O'Connor et al. (19) conducted a multi-center investigation using a standardized phantom to assess the performance of eight different attenuation correction approaches. Knoll et al. (20) found an increase in resolution of up to about 30% for the three vendors using ordered subset expectation maximization (OSEM)-based algorithms. Zeintl et al. (21) demonstrated that modern SPECT/CT technology-enabled very accurate quantitative ^{99m}Tc SPECT imaging in both phantom (error < 3.6%) and patient investigations (error < 1.1%). Seret et al. (22) conducted a study in 2012 to compare the performance of four SPECT/CT systems, the quantitative errors were less than 10%. Hughes et al. (23) also used a phantom to compare the images acquired with three different SPECT/CT systems, and their investigation found no significant difference in the quantification of activity between the systems involved.

These findings highlight a challenge in standardizing SPECT/CT quantification across various nuclear medicine facilities. Therefore, to generate quantitative functional images that are repeatable in the same patient at multiple time points and reproducible across centers and scanners, an absolute quantification reference with a low coefficient of variation is needed to assure harmonization even among the reconstruction methods. Thus, absolute quantification's main merits are uniformity and consistency.

Table 1.1 Main characteristics of the SPECT/CT systems and their own reconstruction algorithms.

System and reconstruction software	SPECT detector	Collimator LEHR	corrections			CT
			Attenuation	Scatter	Resolution Recovery	
GE Discovery NM/CT 670 OSEM* **Evolution for Bone**	3/8 in, NaI Crystal 59 PMT* 40 X 54 cm FOV	86.3 Holes (10^3) 35 mm Hole length 0.2 mm Septal thickness	CT-based	DEW* (115 to 125 keV)	Row convolution with spatial resolution kernel	16 slices/rotation
GE Discovery NM/CT Pro 670 OSEM **Evolution for Bone**	3/8 in, NaI Crystal 59 PMT 40 X 54 cm FOV	863 holes (10^3) 35 mm Hole length 0.2 mm Septal thickness	CT-based			16 slices/rotation
Siemens Symbia Intevo OSEM **Flash 3D**	3/8 in, NaI Crystal 59 PMT 38.7 X 53.3 cm FOV	148 holes (10^3) 24.1 mm Hole length 0.16 mm Septal thickness	CT-based	TEW* (108.5 to 129.5 keV)	Gaussian diffusion method with slabs	16 slices/rotation
Philips Brightview XCT OSEM **Astonish**	3/8 in, NaI Crystal 59 PMT 40 X 54 cm FOV	40.2 holes (10^3) 48 mm Hole length 0.15 mm Septal thickness	CT-based	ESSE*	Convolution with spatial response function	2 slices/rotation

*OSEM ordered subset expectation maximization, PMT photomultiplier tube, DEW dual-energy window method, TEW triple-energy window, ESSE effective source scatter estimation method.

Table 1.2 Major studies that compared the quantitative accuracy of SPECT/CT systems among different vendors and centers

Year	Author's	SPECT/CT	Vendors	Source	Results	Conclusion's
2012	Zeintl et al. (24)	1	Discovery NM/CT 670	^{99m}Tc	3.6% in phantoms and 1.1% of patients	Excellent accuracy with an average quantitative accuracy of 3.6% in phantoms with different-sized spheres and 1.1% in patients with a focus on the bladder.
2012	Hughes et al (23)	3	BrightView, Infinia Hawkeye 4, Symbia-T6	^{99m}Tc	The mean activity error: AST (– 24.0 ± 1.6%); EVB (– 38.0 ± 1.6%); EVC (– 34.5 ±2.3%); FLA (– 33.8 ± 1.6%)	Philips provided the most quantitatively accurate and highest contrast images. Siemens and General Electric provided relatively higher signal-to-noise ratios and more uniform images.
2012	Seret et al (22)	4	Brightview, Discovery NM/CT 670, Infinia Hawkeye 4, Symbia T6,	^{99m}Tc	Error below 10% was achieved.	Quantification seemed to be feasible within 10% error limits in objects. Partial volume effect. correction strategy remains necessary for the smallest structures.
2012	Knoll et al (20)	3	Infinia Hawkeye 4, BrightView, Symbia-T6	^{99m}Tc	16.7% for GE; 30% for Philips; and 26.5% for Siemens	The largest improvement in image resolution and contrast is found for the scatter-corrected slices without post-filtering.
2016	Kangasmaa et al (25)	10	3 GE (Infinia, Optima, Discovery) and 5 Siemens (four Symbias and one Intevo).	^{99m}Tc	The coefficient variations from 19% to 5%	Quantitative SPECT is reproducible in a multi-center setting with third-party reconstruction software.

Table 1.1 (Continued)

Year	Author's	SPECT/CT	Vendors	Source	Results	Conclusion's
2016	Zimmerman et al (26)	10	Symbia T2, T6, T16, Infinia Hawkeye 4, Nucline Spirit DH-V	^{133}Ba and ^{131}I	6% with planar imaging, and 2% for SPECT/CT	The project demonstrated the need for training and standardized protocols to achieve good quantitative accuracy and precision in a multi-center setting.
2017	Nakahara et al (27)	4	Brightview XCT, Discovery NM/CT 670, Infinia Hawkeye 4, Symbia T6	^{99m}Tc	10% for all quantitative metrics.	A digital phantom developed by QIBA would be useful for harmonizing SUVs in multi-center trials using SPECT/CT.
2018	Grošev et al.	4	Siemens Symbia T2	^{133}Ba	SPECT/CT using CT-AC, R=1.00 ±0.08	The results are those obtained within the larger IAEA study and confirm that SPECT/CT method is the most appropriate for accurate activity quantification.
2019	Peters et. al. (28)	5	Discovery NM/CT 670 Pro, Precedence T6, Symbia Intevo, and Symbia T16 (twice)	^{99m}Tc	Inter-system variability was 16% and 17% Standardized reconstruction decreased this variability to 4 and 5%.	Different reconstruction algorithms are the leading cause of the variation between centers. The optimal clinical method for reconstructing quantitative images with five iterations and 15 subsets was obtained with the NM/CT850 gamma camera.

NEMA-IEC National Electrical Manufacturers Association and the International Electrotechnical Commission, QIBA Quantitative Imaging Biomarkers Al

1.3 Structure of the Thesis

1.3.1 Research Questions

The hypotheses to be evaluated by this project are:

(a) how accurate are different SPECT/CT systems with a phantom setup using ^{99m}Tc and ^{131}I radionuclides in terms of quantitative accuracy?

(b) how stable is our local SPECT/CT in terms of the calibration factor over the period of a six-month investigation?

To answer the hypothesis, we assessed the quantitative accuracy using three multi-clinical sites; three SPECT/CT systems; two phantom-based imaging systems; and two radionuclide-based imaging studies.

1.3.2 Research Objectives

The intention of this study is to standardise quantitative SPECT/CT imaging that can be applied regardless of manufacturer, location, and other site-specific characteristics. The aims of this work were:

1. To assess the accuracy of absolute activity quantitation among multi-centers and multi-vendor.

2. To evaluate the current performance of our local SPECT/CT at Institut Perubatan dan Pergigian Termaju (IPPT) in terms of stability.

3. Establish a calibration factor to reconstruct image data, which can be applied to our quantitative SPECT/CT.

1.3.3 Significance of the Study

1. This study is valuable to assess levels of error in activity quantification, thus reducing inter-and-intra-observer variability.

2. To reduce differences in quantitative reads between centers by allowing comparison of parameters in the same patient or between groups, or data from different SPECT/CT systems in different locations.

3. To encourage good practice by implementing optimal standards and readily adjust to changes without losing quality.

1.3.4 Thesis Organization

Chapter 2 of this dissertation provides background on the principle of SPECT imaging, as well as the system performance and image quality in SPECT. Chapter 3 reviews the quantitative accuracy and reproducibility of the SPECT/CT system and the various approaches taken to address the factors that affected activity quantification. Chapter 4 evaluates the absolute activity difference and relative error of the two General Electric Discovery NM/CT 670 systems using ^{99m}Tc in phantom studies. Chapter 5 assesses the quantitative performance of the Symbia Intevo T16 SPECT/CT system using the OS-EM algorithm based on Flash-3D reconstruction software. Chapter 6 assesses the dependences of calibration factor (CF) values over a range of activities and voxel sizes using high activities of ^{131}I. Chapter 7 evaluates the CF stability of our local SPECT/CT at IPPT system over a six-month period. Finally, Chapter 8 an overall conclusion of the complete dissertation.

CHAPTER 2

SINGLE PHOTON EMISSION COMPUTED TOMOGRAPHY / COMPUTED TOMOGRAPHY IMAGING

In this chapter, the complete workflow to generate a SPECT images will be described and reviewed in brief, along with how image quality in SPECT approaches contributes to improving patient outcomes. The organisation of the chapter is as follows: background information, the physics of SPECT, the radionuclides used in SPECT are described, the methodology of SPECT imaging is introduced and related to the physics of SPECT, instrumentation, acquisition, and reconstruction.

2.1 Introduction

SPECT imaging is a 3D volumetric functionality, by rendering and shading, provides cross-sectional images of in vivo radiopharmaceutical distribution (29). The technique has overcome the main limitations of planar imaging, which limited 2D information by projected the 3D distribution onto a single plane (or a single perspective view), that is, right and left, superior and inferior localization, but not anterior and posterior (30). Thus, the main advantage of SPECT is the higher image contrast, which allows for a complete 2π angular sampling to separate activity accumulation in organs that would be superimposed or removed out-of-plane information (Z-depth) in planar images (31). Thus, SPECT reduces the unwanted count contribution in areas of interest from other regions and defines any spatial relationships between neighboring regions. Resulting in improved sensitivity by detecting additional lesions and specificity by excluding sites of physiological tracer uptake (32,33).

SPECT is versatile and clinically effective for adult and paediatric humans due to its high sensitivity and specific activity of radionuclides (34). It can quantify in vivo physiology for a wide range of conditions and applications in the 10^{-10} to 10^{11} radiotracer concentration range, below the threshold of a pharmacological effect (35). SPECT offers many advantages, such as a longer physical half-life radiotracer that can better match biological processes (36). Furthermore, SPECT permits simultaneous imaging of the distribution of multiple tracers, each with different photon emission energies. (37). Given this spectrum, the SPECT can aid in detecting, localizing, diagnosing, staging and restaging of lesions, tumors, disease and organ function for the evaluation of diseases and disorders such as, but not limited to, cardiovascular disease, neurological disorders and cancer. The images produced by the system can also be used by the physician to aid in radiotherapy treatment planning and interventional radiology procedures (36).

2.2 The Physics of SPECT

2.2.1 Radioactive Disintegration Processes

The main radioactive decay processes in nuclear medicine are divided into three categories: alpha (α) decay; beta (β) decay, which includes β^-, β^+, and electron capture and; gamma (γ) decay, which includes isomeric transition and internal conversion. Since the current research mainly relates to the γ-ray process, a discussion will be summarised in this chapter to only γ-ray.

SPECT is based on the physical mechanisms of gamma emission. When an unstable atom undergoes α or β decay by an isobaric transition, it usually produces a daughter nuclide that is in its excited state, then it will further decay to a lower energy level by emitting a gamma photon with low energy in the range of 100 keV to 500 keV

without change of mass and atomic number in order to reach stability. This process, wherein energy is emitted as a gamma photon with the Z and N remaining constant, is called isomeric transition (IT). However, if the nuclear excited state has a long lifetime, it is called a metastable state, in which the only energy emitted from the nucleus is gamma rays. An example of a metastable nuclear isomer is technetium-99m (^{99m}Tc) (38).

2.2.2 Photons Interactions

For any interaction with matter, such as water (equivalent to soft tissue), NaI (SPECT crystal), and lead (SPECT collimator), the γ-ray photon interacts primarily with orbital-electron (e^-) in the atoms, either by a loosely bound electron or by a tightly bound electron. Therefor, based on the energy of radionuclides used in SPECT ($h\nu < 511\ keV$), the momentum transfer during photon-electron interaction is through either photoelectric absorption or Compton-scattering (Fig.2.1) (39).

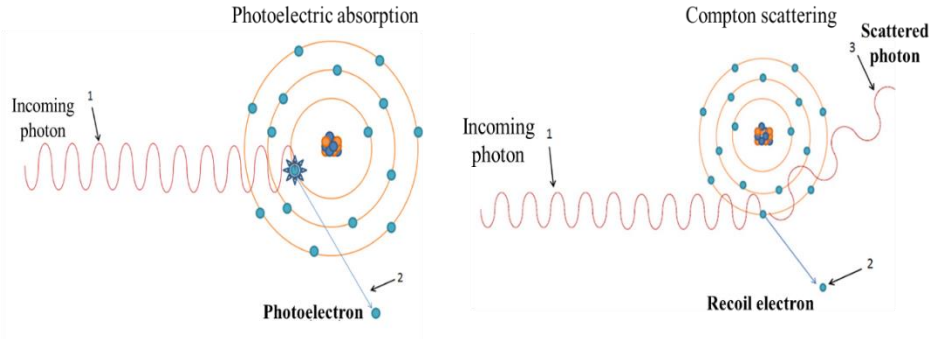

Figure 2.1 Gamma-ray interactions with matter (40).

The photoelectric absorption reflects the interaction of a photon with a tightly bound electron (K-shell) below about 100 keV, where the photon's at the right frequency knocks out an electron, the photon is completely absorbed, and its energy is transferred to the emitted electron (photoelectron). The likelihood of photoelectric

effects depends strongly on the atomic number (Z) and lower photon energies (E) (likelihood ~ Z^3/E^3). Compton scattering reflects the interaction of photons with weakly bound electrons in the range of 100 keV to 10 MeV, where the photon's knocks the electron out, part of the photon energy is transferred to an ejected electron and the photon is scattered at an angle (θ) with a lower frequency (41,42). The likelihood of Compton scattering is linearly dependent on the electron density (e/cm^3), weakly dependent on the energy of the photon (1/E), and independent of Z. Figure 2.2 shows that the photoelectric effect is dominant at lower energies and pair production at higher energies. Compton scattering takes over at medium energies but for low-Z media, such as soft tissue or water.

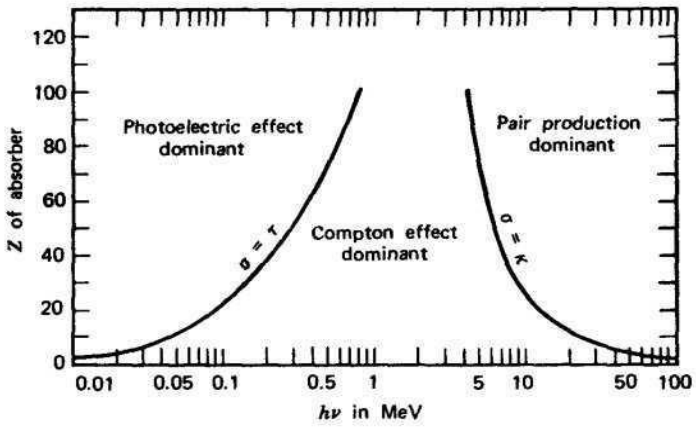

Figure 2.2 Relative importance of Photoelectric effect, Compton scattering and Pair production over an energy of the photons and atomic numbers of the attenuating material (38).

2.2.3 Photon Attenuation

SPECT imaging starts with the injection of activity into the patient for imaging. As a result, the γ-rays beam will undergo various interactions as it passes through the body's, resulting in a change in the flux of the γ-rays defined by *Beer's law* as (43):

$$\Phi = \Phi_0 e^{-\mu x} \qquad \text{(Eq. 1)}$$

$$\Phi = \Phi_0 e^{-\sum_i \mu_i x_i} \qquad \text{(Eq. 2)}$$

Which relates the flux (Φ_0) of an incident monoenergetic γ-rays beam to the flux (Φ) of the same beam after passing through a homogeneous cross-section of thickness (x) (Eq. 1) or a heterogeneous cross-section of thickness (x) (Eq. 2). The flux (Φ) of a γ-ray photons with $h\nu$, will decrease exponentially as a function of the penetration depth (x) due to absorption or scattering out of the beam. The combination of these interactions is the probability that a photon will interact, per unit thickness, at a certain energy. This probability is represented by the total linear attenuation coefficient (μ), given as the sum of the individual linear attenuation coefficients for each type of interaction (38):

$$\mu = \tau + \sigma + \kappa \qquad \text{(Eq. 3)}$$

Where τ, σ, and κ denote, respectively, the linear attenuation coefficients for the photoelectric effect, Compton scattering, and pair production. Table 2.1 shows that the probability of linear attenuation coefficient for each of these types of interaction in H_2O, NaI(Tl), and Pb as a function of 140 keV emitted by ^{99m}Tc.

Table 2.1 Contributions from different interactions to the linear attenuation coefficient for 140 keV photon (44).

	Photoelectric (%)	**Compton (%)**	**Linear attenuation coefficient (cm^{-1})**
H_2O	0.6	97.4	0.154
NaI	77.7	15.3	15.3
Pb	91.1	4.0	26.9

2.3 Administration of a Radioactive Drug to the Patient

The US Food and Drug Administration has legally defined that all radiolabeled compounds or substances used for diagnosis or therapy are radiopharmaceuticals or radioactive drugs (45). A radiopharmaceutical is a chemical combination of a radionuclide and a pharmaceutical. The radionuclide gives off radiation when it decays and can be tracked and measured. Meanwhile, the pharmaceutical is a drug-like[3] substance trapped by given organs based on their metabolic function and preferentially absorbed according to their affinity for the receptor sites (46,47). The radiopharmaceutical can be administered to the patient by injection, inhalation, or ingestion. The radiopharmaceutical is chosen according to its properties (e.g., effective half-life; energy and type of decay emission; oxidation-reduction stability; specific activity; rich coordination chemistry; cost and transportation; and availability and ease of production) (48). However, the radionuclides used in nuclear medicine are classified as diagnostic or therapeutic radionuclides.

Diagnostic radionuclides fall into two categories: a) single photon emitters: emit γ-rays directly from the nucleus, with energies ranging from 70 keV to 360 keV; b) positron emitters: emit pairs of annihilation photons, two γ-rays with a fixed energy of 511 keV, back-to-back at 180° apart. These high-energy photons can penetrate into deeply seated targets, escape from the body, and be measured externally to provide the spatial distribution of the signals in vivo. In contrast, particle-emitting radionuclides like alpha, beta, and Auger electrons are not useful for diagnostic imaging because

[3] Drug-like molecules, according to Dr. Lipinski, refers to compounds that have sufficiently acceptable ADME properties and sufficiently acceptable toxicity properties to survive through the completion of human Phase I clinical tria

they are completely absorbed by the patient's body and are harmful and non-penetrating (49). Figure 2.3 illustrates the types of radioactive decay and their applications in nuclear medicine. The therapeutic radionuclides are beyond the scope of this project.

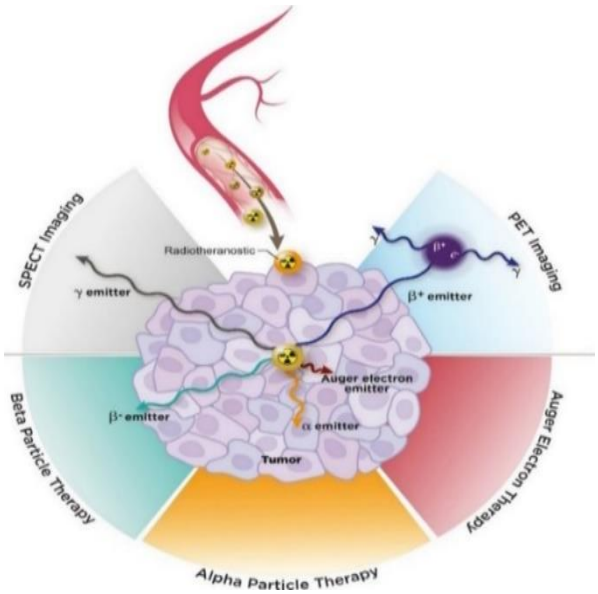

Figure 2.3 Types of radioactive decay and their application's (50).

Technetium-99m ($^{99m}_{43}Tc$) is a common medical radionuclide used in SPECT. It is a pure γ emitter with 140 keV energy, obtained from molybdenum-99 ($^{99}_{42}Mo$) which undergoes an isobaric transition and decays by a β^- emisstion (87%) to the metastable state $^{99m}_{43}Tc$ and the remaining 13% to the ground state technetium-99 ($^{99}_{43}Tc$). The $^{99m}_{43}Tc$ decays by a γ-ray emission of 140 keV to $^{99}_{43}Tc$ via isomeric transition. The gound state $^{99}_{43}Tc$ has a relatively long half-life and decays to a stable ruthenium-99 ($^{99}_{44}Ru$) by β^- emission (51).

$$^{99}_{42}Mo\ (66h) \rightarrow {}^{99m}_{43}Tc\ (6h) + \beta^- + \bar{\nu_e} \qquad \text{(Eq. 5)}$$

$$^{99m}_{43}Tc\ (140\ \text{keV}) \rightarrow {}^{99}_{43}Tc\ (211{,}000\ \text{years}) + \gamma \qquad \text{(Eq. 6)}$$

$$^{99}_{43}Tc \rightarrow {}^{99}_{44}Ru + \beta^{-} + \bar{\nu_e} \qquad \text{(Eq. 7)}$$

The chemical separation of short-lived $^{99m}_{43}Tc$ from long-lived $^{99}_{42}Mo$ is obtained from a chromatographic generator by the principle of an anion exchange column[4] (52). The ideal characteristics of ^{99m}Tc that make it the versatile are: (a) pure γ-ray photon with no primary particle emission, thus avoiding needless radiation to the patient; (b) 140 keV energy, sufficient for it to escape from the patient's body and be easily detected, and suitable for high-efficiency detection using NaI detectors; (c) 6.02 hours half-life, long enough for preparation, injection, uptake, and image acquisition but short enough to excrete and eliminate from the body quickly; (d) high specific activity, make it possible to label with biologically active molecules; and (e) eight oxidation states ranging from -I to VII (-1 to +7), which makes it possible to obtain several different radiopharmaceuticals (52–54).

2.4 SPECT System Design

SPECT is composed of a collimator, scintillation crystal, photomultiplier tubes (PMTs), electronics circuitry, a computer system, and a rotating gantry. This section provides a brief summary of those parts.

2.4.1 SPECT Collimator

Between the detector and the patient, a geometrical collimator is placed in front of the γ-ray camera. Since γ-rays are emitted isotropically and distributed uniformly

[4] In brief, Al_2O_3 and MoO_4^{2-} are polymerized on a sterile glass column. MoO_4^{2-} continual decay leads to the formation of TcO_4^-. $NaCl^-$ is injected into a column, then an ion exchange takes place between the chloride ions and pertechnetate ions, so the ^{99m}Tc is eluted in the form of $Na^{99m}TcO_4^-$.

into 4π steradians[5], without blocked apertures, γ-rays from all directions would be recorded by the detector, giving an image blur. Thus, the collimator is used to determine the directionality of the incoming photons upon the camera's detector for later retrieval of the 3D activity distribution. Hence, The absorption of incident photons by collimator improves spatial resolution and decreases the system sensitivity (55). In clinical practice, the parallel-hole collimator is the collimator of choice due to the optimal image quality offered by such a linear array of apertures, where the resolution depends on the perpendicular distance from the point source to the detector while the sensitivity is equal everywhere in the FOV, as illustrated in (Fig. 2.4). The parallel-hole collimator is used to collimate and filter a photon stream, and absorb secondary photons scattered by an object (56). However, the performance of a parallel-hole collimator is influenced by its geometry (i.e., hole length, hole diameter, and septal thickness), which has effects on the image quality, spatial resolution, and system sensitivity (56).

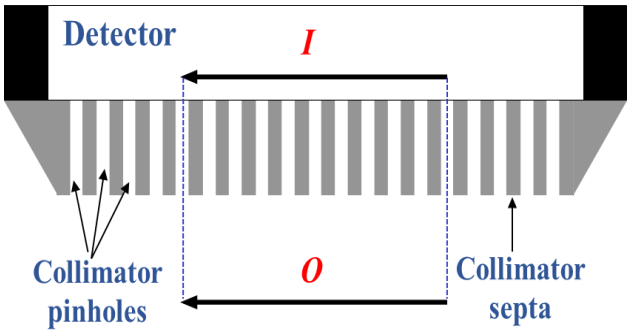

Figure 2.4 Illustration a parallel-hole collimator.

[5] Steradians is the SI unit of a solid angle $= \frac{sphere\ area\ (A)}{sphere\ radius\ (r^2)} = \frac{4\pi r^2}{r^2} = 4\pi$

2.4.2 Scintillation Detector

The scintillation crystal used in SPECT is typically thallium-activated sodium iodide, NaI(Tl). In brief, the process is as follows: a light-quanta emitted isotropically at the crystal, upon γ-quanta absorption; an secondary electrons generated at the cathode of the PMT, in response to an incident light-quanta; the amount of secondary electrons becomes the amount of current at the anode, by means of electron multiplier (a cascade of positive dynodes) (Fig. 2.5). The output current from the anode is then matched, shaped, and amplified by a preamplifier and amplifier, sorted by a PHA, and then registered as a count, carrying information about the photon energy and spatial coordinates x and y related to the position of the photon emission. The data is then fed to a computer for image processing, display, and storage, which in turn reflects the spatial distribution of the emitted photons (57).

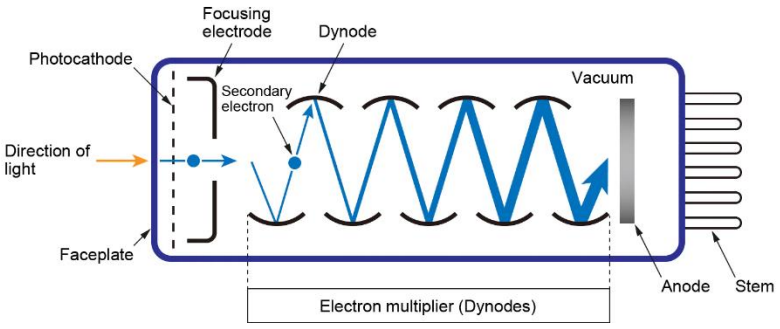

Figure 2.5 Illustration of the photomultiplier tube (58).

2.4.3 Rotating Gantry

The function of the rotating gantry in SPECT is to create a plurality of planar images around the object in order to increase the number of lines along which γ-rays can be detected simultaneously. Thus, the sensitivity of the imaging process is drastically increased. However, the collimator and the detector are mounted on a pair of heads supported by the rotating gantry. The longitudinal axis of the gantry and the

long axis of the patient's table are perpendicular. The dual-detector heads rotates around the patient's long axis at small angle increments (3º-6º) for 180º or 360º angular sampling (Fig. 2.6). The flexibility of the gantry movements allows estimating the target volumes and the distribution of radiopharmaceuticals within these volumes (e.g., the spatial distribution of flow in lymphatics) (59).

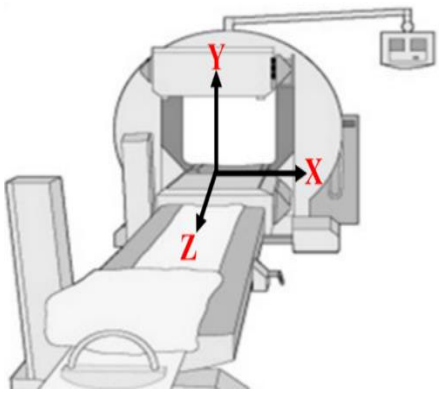

Figure 2.6 SPECT scanner scan along the axial direction (Z-axis), parallel to the long axis of the patient. Y-axis is perpendicular to the patient. X-axis runs side-side of the patient.

The gantry allows the camera to move in a circular orbit with a fixed radius of rotation of the camera heads or follow the body contour (elliptical orbit). Following the body contour improves spatial resolution and slightly improves detection efficiency. The detectors could be set at: 180º parallel, in which the two heads are placed on diametrically opposite sides of the axis of rotation, or 90º perpendicular, in which the two detector heads are placed at adjacent edges orthogonal to each other, reducing the attenuation and depth-dependent losses in spatial resolution for cardiac SPECT. The SPECT acquistion are available in three modes: step-and-shoot, continuous, and step-and-shoot continuous. In step-and-shoot mode, the projection data are acquired only when the detector is stationary at sequential views. In the continuous mode, data are acquired as the detector moves continuously at constant

speed. Whereas in the step-and-shoot continuous mode, data are acquired both when the detector is stationary and when the detector moves from one view to the next. During the step-and-shoot continuous mode, the counts acquired during the 6° rotation are partitioned as follows: between 0° and 3°, counts are assigned in position 0°, and between 3° and 6°, they are integrated in the next position 6° (Fig. 2.7) (60,61).

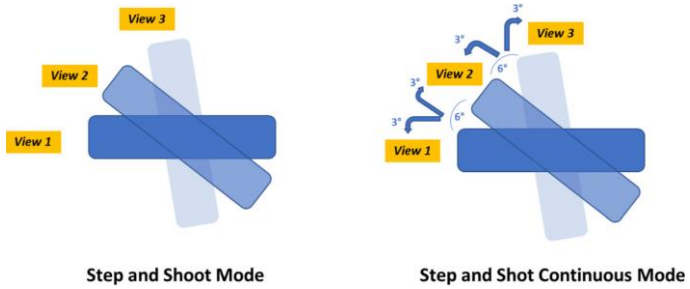

Figure 2.7 An illustration of step-and-shoot versus step-and-shoot continuous mode acquisition (62).

2.5 Projection and Reconstruction of the Radioactivity Distribution

In SPECT, projection is the process of recording the γ-flux from an object through an collimator and onto a detector from a single plane at a qiven angle or from multiple coplanar (different views/angels**)**. Meanwhile, "reconstruction" is the process of mathematically assembling several projections together to obtain information along the depth of the object (i.e., underlying distribution). Since the goal of SPECT is to measure the spatial and temporal distribution of a radiotracer perfused in a patient's body, the detector heads need to rotate around the patient to obtain projections data from different angles, and the sequence of projections needs to be reconstructed in order to obtain a 3D image.

2.5.1 Image Projection and Sinogram (Detection)

All nuclear images require a certain number of counts obtained in a specific period of time. The term counts or events refers to the number of photons emitted by radionuclides and detected by a scintillation detector. Therefore, the intensity in the pixels is the line-integrated photon counter and time-integrated signal detected within the energy window. A short description of the Poisson distribution, image projection in SPECT and sampling completeness will be discussed in this section.

2.5.1(a) Probability of Detected Photons

Radioactive decay is a stochastic process (random process), and the decay is governed by the laws of quantum physics (63). The detectors (both X-ray and γ-ray) are 'photon counting', and there are always fluctuations in photon counts. Thus, the detection of individual γ-quanta are random events, and the pixel values are random (64). The Poisson distribution gives the probability of a photon passing through the imaged object unchanged by (51):

$$p(k) = \frac{q^k e^{-q}}{k_i} \qquad \text{(Eq. 8)}$$

Where **q** is an expected events (i.e., the number of photons emitted by the γ-ray source) and **k** is an detecting events (i.e., the number of photons measured by the detector**).** The Poisson process can be approximated by a Gaussian distribution and the standard deviation of the Poisson distribution is calculated as $\sqrt{q}$.